Guo *et al. Biochar* (2026) 8:40
https://doi.org/10.1007/s42773-025-00558-9

Biochar

ORIGINAL RESEARCH Open Access

# Divergent legacy effects of biochar on nitrous oxide emissions in acidic soils driven by altered microbial N pathways

Shumin Guo[1,2], Haiyan Lin[1,2], Zhutao Li[1,2], Zhaoqiang Han[1,2,3], Jie Wu[1,2], Xiaomeng Bo[1,2], Mengxue Shen[1,2], Zhiwei Zhang[1,2], Shuwei Liu[1,2,3], Jinyang Wang[1,2,3*] and Jianwen Zou[1,2,3]

## Abstract

Acidic soils are global hotspots of nitrous oxide ($N_2O$) emissions, and biochar has been proposed as a promising mitigation strategy. However, most current evidence comes from short-term studies, and the legacy effects and underlying mechanisms remain poorly understood. Here, we collected acidic soil samples from three sites with and without biochar application, representing short-term (3 and 5 years) and long-term (9 years) legacy effects. Using microcosm incubations, isotope-based source partitioning, and microbial analyses, we evaluated $N_2O$ dynamics and their microbial drivers. The short-term legacy effects of biochar significantly reduced $N_2O$ emissions by inhibiting gross $N_2O$ production and enhancing $N_2O$ reduction. This was primarily attributed to reduced nitrification-derived $N_2O$, increased *nosZ* gene abundance, and enrichment of taxa carrying the *nosZ* gene, such as *Rhodanobacter* and *Gemmatimonas*. In contrast, long-term legacy effects markedly increased $N_2O$ emissions because biochar suppressed $N_2O$ reduction more strongly than its production. This was linked to reduced *nosZ* abundance, increased fungal denitrification, and depletion of dissolved organic carbon and denitrifying bacteria. Together, these findings reveal that the legacy effects of biochar on $N_2O$ emissions diverge over time, driven by changes in microbial nitrogen cycling pathways. These results underscore the importance of incorporating temporal and microbial perspectives when evaluating the long-term climate impacts of biochar and developing sustainable soil management strategies.

## Highlights

- Biochar shows contrasting legacy effects on $N_2O$ emissions
- Biochar reduces $N_2O$ emissions by suppressing production and enhancing reduction
- Biochar increases $N_2O$ emissions by inhibiting reduction more than production
- Biochar enriches *Rhodanobacter* and *Gemmatimonas* carrying the *nosZ* gene

**Keywords** Acidic soils, Biochar, Legacy effects, Nitrous oxide, Isotopocule analysis, Functional genes

*Correspondence:
Jinyang Wang
jywang@njau.edu.cn
Full list of author information is available at the end of the article



Springer

**Graphical Abstract**

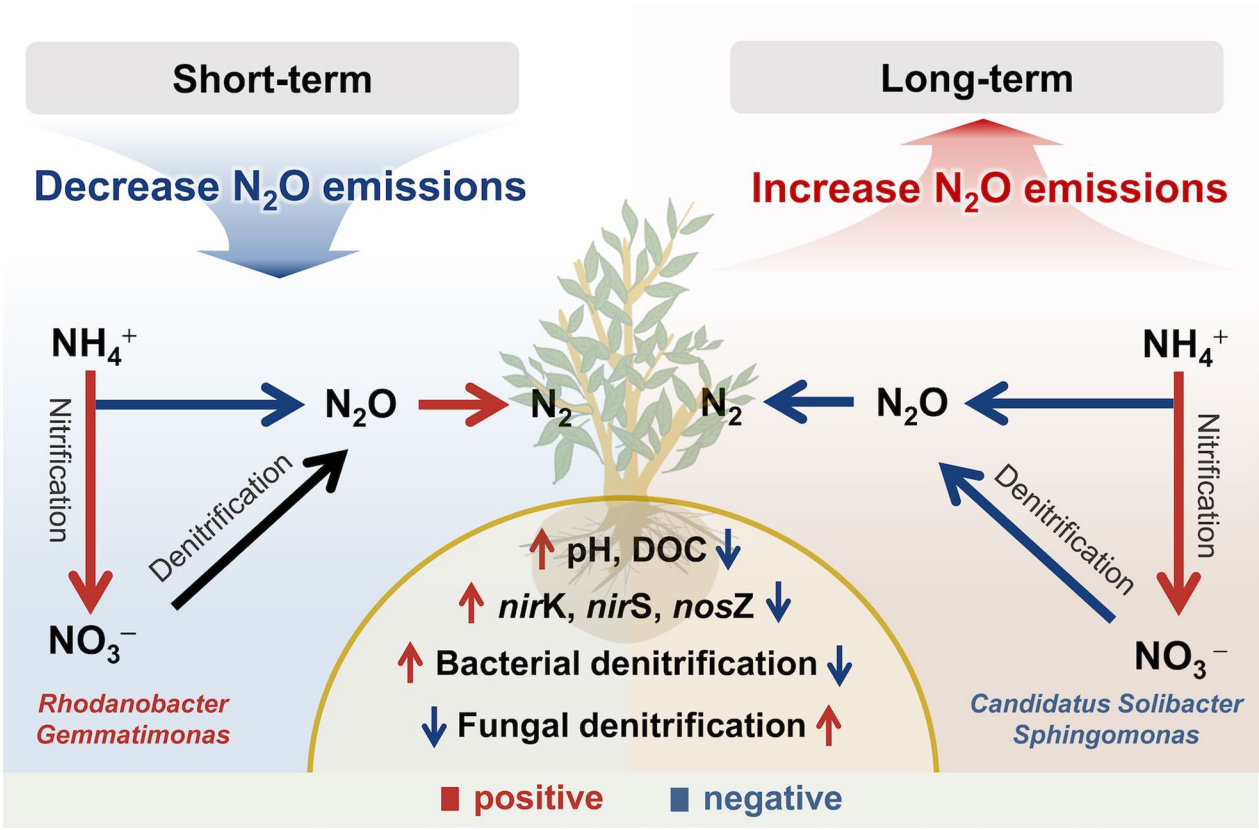


## 1 Introduction

Nitrous oxide ($N_2O$) is a long-lived greenhouse gas and a major contributor to stratospheric ozone depletion, playing a critical role in global climate change (Ravishankara et al. 2009). Agricultural soils represent the dominant source of anthropogenic $N_2O$ emissions worldwide (Tian et al. 2020), with acidic soils recognized as emissions hotspots due to their higher emission intensities under equivalent nitrogen (N) input and greater sensitivity to fertilization (Wang et al. 2018). The continuous use of synthetic N fertilizers, driven by increasing food demand and population growth, is likely to further exacerbate acidification in acidic soils and consequently intensify $N_2O$ emissions. Therefore, the development of effective and sustainable mitigation strategies for acidic soils is essential to support global climate goals.

Biochar, a carbon-rich material derived from pyrolyzed biomass, has attracted growing attention for its potential to sequester carbon and reduce greenhouse gas emissions in agroecosystems (Woolf et al. 2016). In acidic soils, biochar has been widely reported to reduce $N_2O$ emissions by improving aeration, raising pH, altering substrate availability, absorbing $N_2O$, and inhibiting nitrification and denitrification (Xu et al. 2014; Krause et al. 2018; Duan et al. 2019; Bo et al. 2023). However, inconsistent outcomes have also been reported, including neutral or even stimulatory effects (Ameloot et al. 2013; Wang et al. 2016; Lin et al. 2017). These discrepancies are often attributed to variations in soil properties, climate, vegetation, and biochar characteristics (Cayuela et al. 2014).

Importantly, biochar is highly stable in soils and can persist for decades (Chen et al. 2019), making its long-term effects more relevant for climate mitigation. Over time, aging processes, including microbial activity and abiotic weathering, can alter biochar's physical and chemical properties, such as reducing porosity, increasing surface acidity, and diminishing adsorption capacity (Dong et al. 2017; Wang et al. 2020). These changes may modify how biochar interacts with N transformation processes and challenge the assumption that its mitigation effects remain stable over time. Indeed, previous studies

have reported long-term effects of biochar on $N_2O$ emissions, with contradictory results including sustained suppression (Hagemann et al. 2017; Liao et al. 2021; Wang et al. 2021), negligible effects (Han et al. 2021; Guo et al. 2022), or even enhanced emissions (Duan et al. 2018). Despite these insights, the mechanisms underlying such temporal divergence, particularly the role of microbial N cycling, remain poorly understood.

In this study, we investigated the legacy effects of biochar on $N_2O$ emissions in acidic soils and aimed to elucidate the microbial mechanisms underlying these effects. We collected soil samples from three field sites where biochar had been applied for 3, 5, and 9 years, thereby enabling us to examine both short- and long-term legacy effects. We hypothesized that biochar would suppress $N_2O$ emissions in the short term but stimulate them in the long term. This temporal shift likely occurs because biochar can initially mitigate emissions by inhibiting $N_2O$ production and enhancing its reduction, whereas over time it may increase emissions by suppressing $N_2O$ reduction.

## 2 Materials and methods

### 2.1 Site description and soil sample collection

Three field experiments were established in Jiangsu Province, China, all located in tea plantations with a subtropical monsoon climate. Two field experiments were carried out in Jurong, Zhenjiang City (31°58′N, 119°08′E; Alisol), from November 2020 to November 2023 (S1), and from August 2018 to August 2020 (S2). The third experiment was located in Yixing, Wuxi City (31°14′N, 119°46′E; Planosol) from October 2014 to October 2016 (S3). The mean annual temperature and precipitation were 17.1 °C and 1064 mm in Jurong, and 17 °C and 1208 mm in Yixing. Basic soil properties before the experiment are provided in Table S1.

Each site included two treatments with three replicates: conventional N fertilizer (F) and conventional N fertilizer combined with biochar (F + BC). At S1, N was applied at 450 kg N $ha^{-1}$ $year^{-1}$, including 360 kg N $ha^{-1}$ $year^{-1}$ from compound fertilizer (N: $P_2O_5$: $K_2O$ = 16:16:16) and 90 kg N $ha^{-1}$ $year^{-1}$ from cattle manure. At S2 and S3, N rates were 400 and 300 kg N $ha^{-1}$ $year^{-1}$, respectively, using the same compound fertilizer. At all sites, 25% of total N was applied as basal fertilizer and the remainder as topdressing. At all three sites, biochar was co-applied with the basal fertilizer and supplied by Sanli New Energy Company (Shangqiu, Henan, China). The basic properties of biochar are presented in Table S1. At S1, 20 t $ha^{-1}$ of peanut shell biochar was applied in 2020; at S2, the same amount of wheat straw biochar was applied in 2018, and at S3, wheat straw biochar was applied in both 2014 and 2015. At all three sites, other field management practices, such as tea harvesting, leaf trimming, and weeding, were carried out in accordance with the local tea plantation management regime throughout the experimental period.

In November 2023, soil samples were collected from both F and F + BC treatments at each site. Samples were transported to the laboratory on ice in polyethylene bags, sieved (2 mm) to remove roots and debris, and homogenized. Subsamples were stored at 4 °C for physicochemical analysis, frozen at − 80 °C for DNA extraction, or used directly in the microcosm incubation.

### 2.2 Soil microcosm experiment

A microcosm incubation experiment was conducted to investigate the legacy effects of biochar on soil $N_2O$ emissions. Given that net $N_2O$ emissions reflect the balance between microbial production and consumption, we employed the acetylene ($C_2H_2$) inhibition method to differentiate gross $N_2O$ production and consumption (Lin et al. 2022). Three headspace treatments were established for both the F and F + BC soils: (1) 0% v/v $C_2H_2$ (no inhibition), (2) 0.01% v/v $C_2H_2$ (inhibits nitrification), and (3) 10% *v/v* $C_2H_2$ (inhibits both nitrification and $N_2O$ reduction). Each treatment was performed in triplicate. Briefly, 20 g (dry weight equivalent) of freshly sieved soil was placed into 120 mL serum bottles and preincubated at 25 °C with 55% water-holding capacity (WHC) for 7 days to revive and stabilize microbial activity. After preincubation, urea was added at a rate of 100 mg N $kg^{-1}$ dry soil, and soil moisture was adjusted to 70% WHC. The bottles were then sealed with butyl stoppers and exposed to the designated $C_2H_2$ concentrations. Incubation was conducted at 25 °C for 36 days. To maintain aerobic conditions and preserve the experimentally designed conditions, the bottles were ventilated every 1–2 days and replenished with deionized water and $C_2H_2$ as needed.

Gas samples were collected from the headspace on days 1, 3, 5, 7, 9, 12, 16, 22, 30, and 36. After each sampling, bottles were ventilated for 30 min, resealed, and re-equilibrated with the corresponding $C_2H_2$ concentration. Gross $N_2O$ production and consumption were calculated as follows (Yang et al. 2011; Yin et al. 2020; Lin et al. 2022):

$$\text{Gross } N_2O \text{ consumption} = G_{10\%} - G_{0.01\%} \quad (1)$$

$$\text{Gross } N_2O \text{ production} = G_{10\%} - G_{0.01\%} + G_{0\%} \quad (2)$$

where $G_{0\%}$, $G_{0.01\%}$, and $G_{10\%}$ denote the cumulative $N_2O$ emissions measured under 0%, 0.01%, and 10% v/v $C_2H_2$ treatments, respectively. Specifically, the $G_{0\%}$ reflects the net $N_2O$ emissions, i.e., the balance between gross $N_2O$ production and consumption.

### 2.3 Determination of $N_2O$ emission, isotope analysis, and $N_2O$ source partitioning

$N_2O$ concentrations were determined using a gas chromatograph (Agilent 7890A, USA) equipped with an electron capture detector (ECD) operating at 330 °C, calibrated against a standard $N_2O$ gas at 600 ppb (Zou et al. 2009). Cumulative $N_2O$ emissions were calculated by integrating daily fluxes using the trapezoidal rule.

To characterize $N_2O$ production pathways and reduction processes, isotope approaches were performed on gas samples collected at the peak of $N_2O$ emissions for the 0% v/v $C_2H_2$ treatment (Toyoda et al. 2017; Yu et al. 2020). The isotope signatures of $N_2O$, including $\delta^{15}N^{bulk}$, $\delta^{15}N^{\alpha}$, and $\delta^{18}O$, were measured using an isotope ratio mass spectrometer (Isoprime 100, Elementar, UK). The details of isotope measurements and calibration have been previously described (Toyoda and Yoshida 1999; Heil et al. 2015). The $\delta^{15}N^{\alpha}$, $\delta^{15}N^{\beta}$, $\delta^{15}N^{bulk}$, $\delta^{15}N^{SP}$, and $\delta^{18}O$ values of $N_2O$ were calculated as follows (Coplen 2011; Toyoda et al. 2011):

$$\delta^{15}N^{i} = \frac{^{15}N^{i}_{sample}}{^{15}N^{i}_{standard}} - 1 (i = bulk, \alpha, \text{ or } \beta) \quad (3)$$

$$\delta^{18}O = \frac{^{18}O_{sample}}{^{18}O_{standard}} - 1 \quad (4)$$

$$\delta^{15}N^{bulk} = \frac{\delta^{15}N^{\alpha} + \delta^{15}N^{\beta}}{2} \quad (5)$$

$$\delta^{15}N_{SP} = \delta^{15}N^{\alpha} - \delta^{15}N^{\beta} \quad (6)$$

where $^{15}N^{i}$ and $^{18}O$ denote the isotopic ratios of $^{15}N/^{14}N$ and $^{18}O/^{16}O$, respectively. The δ value is expressed as the permil (‰) deviation relative to atmospheric $N_2$ ($^{15}N$) and Vienna Standard Mean Ocean Water ($^{18}O$) for N and oxygen, respectively. $\delta^{15}N^{\alpha}$ and $\delta^{15}N^{\beta}$ indicate the $^{15}N/^{14}N$ isotope ratios at the central ($^{14}N$-$^{15}N$-$^{16}O$) and the terminal ($^{15}N$-$^{14}N$-$^{16}O$) sites in the $N_2O$ molecule, respectively (Yamamoto et al. 2014).

The $N_2O$ isotope signatures of gas samples were measured from both soil-emitted gas and ambient air. The isotope signatures of soil-emitted $N_2O$ were corrected according to mass conservation (Well et al. 2006):

$$\delta_{soil-emitted} = \frac{(\delta_{sample} \times C_{sample} + \delta_{ambient} \times C_{ambient})}{(C_{sample} - C_{ambient})} \quad (7)$$

where δ denotes the isotopic signature and C represent the concentration of the $N_2O$ pool in gas samples and ambient air. The ambient $N_2O$ concentration in the laboratory air was 307 ppb. The $\delta^{18}O$ of soil water ($\delta^{18}O$-$H_2O$) was also measured using an isotope water vapor analyzer (L115-I, Picarro Inc., USA), and was − 4.43‰, − 5.71‰, and − 5.66‰ for the S1, S2, and S3 sites, respectively.

The three-dimensional $N_2O$ isotopocule model (3DIM) was employed to partition microbial sources of $N_2O$ and estimate the $N_2O$ reduction ratio (Lewicka-Szczebak et al. 2020). The 3DIM model used a stable isotope mixing model within a Bayesian framework to estimate the four microbial pathways of $N_2O$ production, including nitrification, nitrifier denitrification, bacterial denitrification, and fungal denitrification. This model relies on the simultaneous use of $\delta^{15}N^{bulk}$, $\delta^{15}N^{SP}$, and $\delta^{18}O$. Two $N_2O$ mixing-reduction scenarios were evaluated as follows: (1) Reduction-Mixing scenario (Scenario 1): the $N_2O$ produced by bacterial denitrification is first reduced, and the remaining unreduced $N_2O$ is then mixed with $N_2O$ produced by other pathways; and (2) Mixing-Reduction scenario (Scenario 2): the $N_2O$ produced by various pathways is first mixed and subsequently reduced. In the model, the isotopic fractionation factors and endmember ranges for nitrification, nitrifier denitrification, bacterial denitrification, fungal denitrification, and $N_2O$ reduction are presented in Table S2. Additionally, the endmember ranges for the four microbial pathways of $N_2O$ production and $N_2O$ reduction were used as prior information in the 3DIM model. For the Bayesian framework, a flat Dirichlet distribution was assigned as the prior distribution for microbial pathway contributions, while a Uniform distribution was used as the prior for the ratio of $N_2O$ reduction. The contributions of microbial pathways to $N_2O$ production and the $N_2O$ reduction ratio were determined using the stable isotope Fractionation And Mixing Evaluation (FRAME) based on the Markov-Chain Monte Carlo algorithm (Lewicki et al. 2022).

Additionally, the $\delta^{15}N^{SP}$-$\delta^{18}O$ mapping approach (SP/O MAP) was applied to estimate the contributions of microbial pathways to $N_2O$ production and reduction ratio (Wu et al. 2019; Lewicka-Szczebak et al. 2020). In the method, nitrification and fungal denitrification, both characterized by high $\delta^{15}N^{SP}$ and $\delta^{18}O$ values, were grouped together, while bacterial denitrification and nitrifier denitrification with low $\delta^{15}N^{SP}$ and $\delta^{18}O$, formed a group (Buchen et al. 2018). Two scenarios of $N_2O$ mixing and reduction were evaluated in this model. The detailed parameters for the model are presented in Table S2. The detailed method used to calculate the contributions of $N_2O$ production pathways and the $N_2O$ reduction ratio was described previously (Wu et al. 2019).

### 2.4 Measurement of soil characteristics

Soil bulk density was measured at a depth of 5 cm using the core method. Soil moisture content was determined by oven-drying fresh soil at 105 °C for 24 h. Soil pH was measured in a 1:2.5 (w/v) soil-to-water suspension using a pH detector (PHS-3C, Shanghai Kangyi, China). Total carbon (TC) and total nitrogen (TN) contents were analyzed using a C/N elemental analyzer (multi EA® 5000, Analytik Jena, Germany). Soil ammonium ($NH_4^+$-N) and nitrate ($NO_3^-$-N) concentrations were extracted using 2 M KCl and measured by continuous flow analysis (Skalar SAN$^{plus}$, Netherlands). Dissolved organic carbon (DOC) was extracted using ultrapure water and determined using a TOC/TN analyzer (multi N/C® 3100, Analytik Jena, Germany).

### 2.5 Determination of potential nitrification and denitrification

Potential nitrification rate (PNR) and the associated $N_2O$ production rate were measured using a modified shaken slurry method (Hart et al. 1994). To distinguish the contributions of different nitrifying groups, selective chemical inhibitors were used: 1-octyne to inhibit ammonia-oxidizing bacteria (AOB) and $C_2H_2$ to inhibit both ammonia-oxidizing archaea (AOA) and AOB (Hink et al. 2017). For each treatment (F and F + BC), three inhibitor setups were established: (a) control (no inhibitor), (b) 1-octyne (0.009% v/v), and (c) $C_2H_2$ (0.013% v/v). Freshly sieved soils (3 g dry weight equivalent) were placed into 120 mL serum bottles, followed by the addition of 20 mL phosphate buffer containing $(NH_4)_2SO_4$ (100 mg N $kg^{-1}$ dry soil). Bottles were sealed with aluminum caps and butyl stoppers, and the designated inhibitors were injected (Mushinski et al. 2019). All samples were incubated in the dark at 25 °C with shaking at 200 rpm for 24 h. At 0 and 24 h, soil slurry was collected for the determination of $NO_3^-$-N, whereas headspace gas was collected for $N_2O$ concentration measurements. PNR and $N_2O$ production from nitrification were calculated based on the changes in $NO_3^-$-N and $N_2O$ concentrations over the incubation period.

Potential denitrification rate (PDR) and denitrification end-product ratio [$N_2O/(N_2O + N_2)$] were measured using the $C_2H_2$ inhibition technique (Carter and Gregorich, 2007; Jones et al. 2022). Briefly, 3 g of fresh soil was placed into 25 mL glass flasks and amended with 3 mL of a solution containing glucose (500 μg C $g^{-1}$ soil) and $KNO_3$ (50 μg N $g^{-1}$ soil). Flasks were divided into two groups: one received 10% v/v $C_2H_2$ to block $N_2O$ reduction to $N_2$, while the other received helium gas as a control. All flasks were incubated in the dark at 25 °C for 5 h. Headspace gas was sampled after incubation, and $N_2O$ concentrations were measured. PDR was estimated based on $N_2O$ production in the $C_2H_2$-treated flasks, and the $N_2O/(N_2O + N_2)$ ratio was calculated from the difference in $N_2O$ accumulation between inhibited ($C_2H_2$) and uninhibited (helium gas) treatments.

### 2.6 Quantitative PCR, amplicon sequencing, and microbial co-occurrence network analysis

Genomic DNA was extracted from 0.25 g of fresh soil using the DNeasy PowerSoil Kit (QIAGEN, Germany) following the manufacturer's instructions. The abundances of bacterial 16S rRNA and N-cycling genes was quantified using the high-throughput SmartChip quantitative PCR technique (HT-qPCR). Primer sequences and amplification protocols for the target genes were adopted from Zheng et al. (2018).

Bacterial community composition was analyzed using Illumina MiSeq sequencing. The V3–V4 region of the bacterial 16S rRNA gene was amplified using the primer pair 341F (5'- CCTAYGGGRBGCASCAG-3') and 806R (5'-GGACTACNNGGGTATCTAAT-3'). PCR products were purified, quantified, and sequenced on the Illumina MiSeq platform (Shanghai BIOZERON Co., Ltd.). Raw sequence data were processed using QIIME 2.0, including primer trimming, quality filtering, denoising, and chimera removal (Callahan et al. 2016). Amplicon sequence variants (ASVs) were generated from high-quality reads for the downstream analyses.

Bacterial co-occurrence networks were constructed separately and analyzed for each site using the Molecular Ecological Network Analysis Pipeline (http://ieg4.rccc.ou.edu/MENA/). Only ASVs with a relative abundance > 0.01% were included in the analysis. The resulting networks were visualized using Gephi (https://gephi.org/). Major ecological modules (subnetworks with > 20 nodes) were identified and selected for further analysis. The relative abundance of each module was calculated as the average standardized relative abundances (z-score) of all ASVs within the module (Delgado-Baquerizo et al. 2018). All sequence data were deposited in the NCBI SRA database under accession number PRJNA1267288.

### 2.7 Statistical analyses

All statistical analyses and figure plotting were performed in R v4.1.1 (R Core Team 2021). Data normality and homogeneity of variance were tested using the Shapiro–Wilk test and Bartlett's test, respectively. At each site, differences between the F and F + BC treatments were evaluated using Student's *t*-test ($P < 0.05$) for the following variables: soil properties, $N_2O$ emissions, PNR, nitrification-driven $N_2O$ production, PDR, $N_2O/(N_2O + N_2)$ ratio, bacterial alpha diversity, the abundances of 16S rRNA and N-cycling genes, and relative abundances of major network modules. Spearman's rank correlation

was used to assess the relationships between cumulative $N_2O$ emissions and the relative abundances of microbial modules. Modules that showed significant treatment effects and strong correlations with $N_2O$ emissions were selected for further genus-level analysis. Differences in the top 10 most abundant genera within the target modules were assessed using STAMP analysis. Spearman's rank correlation was also used to examine the relationships between differentially abundant genera and soil properties, N-cycling gene abundances, and $N_2O$-related processes.

## 3 Results

### 3.1 Soil physicochemical properties

Biochar application induced notable changes in soil physicochemical properties across the three sites (Table 1). At the S1 site (3 years after biochar application), soil pH, TC, DOC, and the C/N ratio significantly increased, while concentrations of $NH_4^+$-N and $NO_3^-$-N decreased markedly. At the S2 site (5 years after application), biochar significantly increased TC, TN, moisture content, DOC, and $NO_3^-$-N concentration, but reduced soil pH and $NH_4^+$-N concentration. Slight decreases in bulk density and the C/N ratio were also observed. At the S3 site (9 years after application), biochar led to significant increases in TC, C/N ratio, and $NO_3^-$-N concentration, while soil pH, TN, DOC, and $NH_4^+$-N concentration declined. Bulk density and moisture content showed no significant differences between treatments.

### 3.2 $N_2O$ emissions

The legacy effects of biochar significantly altered soil $N_2O$ emissions across all three sites (Fig. 1). Temporal patterns of $N_2O$ fluxes were consistent among treatments, with emissions occurring within the first two weeks of incubation, followed by a gradual decline (Fig. 1a, c, e). At the S1 and S2 sites, biochar significantly reduced cumulative $N_2O$ emissions by 41% and 84%, respectively. In contrast, at the S3 site, biochar markedly increased cumulative $N_2O$ emissions by fourfold. Across all sites, biochar inhibited gross $N_2O$ production (Fig. 1b, d, f). However, biochar substantially increased gross $N_2O$ consumption and the ratio of gross $N_2O$ consumption to production at the S1 and S2 sites, but notably reduced both at the S3 site. Moreover, at the S3 site, biochar reduced gross $N_2O$ production and consumption by 32% and 68%, respectively. This indicates that biochar had a stronger inhibitory effect on $N_2O$ reduction than on $N_2O$ production.

### 3.3 $N_2O$ source partitioning and reduction

The legacy effects of biochar altered the relative contributions of microbial pathways to $N_2O$ production and the extent of $N_2O$ reduction, with consistent patterns observed across scenarios 1 and 2 (Figs. 2 and S1). According to the 3DIM model, bacterial denitrification was the dominant source of $N_2O$ across all samples, followed by nitrifier denitrification, fungal denitrification, and nitrification (Fig. 2b). Biochar consistently reduced the contribution of nitrification across all sites. At the S1 and S2 sites, biochar increased the contribution of bacterial denitrification, reduced that of fungal denitrification, and increased $N_2O$ reduction ratio, whereas biochar had the opposite effects at the S3 site. The SP/O MAP results showed that bacterial denitrification and fungal denitrification were the dominant contributors to soil $N_2O$ production (Fig. S1b). Biochar increased both the $N_2O$ reduction ratio and the contributions of bacterial denitrification and fungal denitrification at the S1 and S2 sites, while both metrics declined following long-term application at the S3 site. Furthermore, the 3DIM model and the SP/O map showed good agreement in the extent of $N_2O$ reduction under scenarios 1 and 2, and both models

**Table 1** The physicochemical properties of soil under different treatments

| | S1 | | S2 | | S3 | |
|---|---|---|---|---|---|---|
| | F | F + BC | F | F + BC | F | F + BC |
| Bulk density (g $cm^{-3}$) | 1.03 ± 0.09 | 1.08 ± 0.11 | 1.02 ± 0.03 | 1.07 ± 0.11 | 1.05 ± 0.08 | 0.94 ± 0.08 |
| pH | **4.38 ± 0.01** | **4.47 ± 0.01** | **4.42 ± 0.00** | **4.35 ± 0.01** | **4.13 ± 0.02** | **4.02 ± 0.01** |
| SOC (g $kg^{-1}$) | **42.85 ± 0.65** | **52.45 ± 0.15** | **35.75 ± 0.15** | **58.96 ± 0.64** | **31.37 ± 0.69** | **43.93 ± 0.66** |
| TN (g $kg^{-1}$) | 1.84 ± 0.06 | 1.97 ± 0.02 | **1.53 ± 0.02** | **2.39 ± 0.04** | **1.41 ± 0.06** | **1.13 ± 0.01** |
| Moisture (%) | 43.73 ± 1.59 | 46.70 ± 0.67 | **25.55 ± 0.11** | **38.02 ± 1.32** | 28.00 ± 0.00 | 30.00 ± 0.00 |
| DOC (mg $kg^{-1}$) | **88.04 ± 0.64** | **101.89 ± 0.83** | **84.02 ± 0.19** | **115.37 ± 0.68** | **54.05 ± 2.22** | **27.89 ± 0.72** |
| C/N ratio | **27.20 ± 0.59** | **31.12 ± 0.23** | 27.27 ± 0.31 | 28.84 ± 0.75 | **25.94 ± 0.70** | **45.22 ± 0.51** |
| $NH_4^+$ (mg N $kg^{-1}$) | **29.20 ± 0.28** | **24.07 ± 0.32** | 13.53 ± 0.58 | 11.94 ± 0.35 | **19.06 ± 0.97** | **10.94 ± 0.56** |
| $NO_3^-$ (mg N $kg^{-1}$) | **20.58 ± 0.31** | **16.48 ± 0.00** | **20.04 ± 0.13** | **22.47 ± 0.05** | **18.44 ± 0.01** | **40.77 ± 0.22** |

Values indicate means ± SE ($n = 3$). Values in bold represent statistically significant differences ($P < 0.05$) between treatments. F, conventional N fertilizer; F + BC, conventional N fertilizer combined with biochar

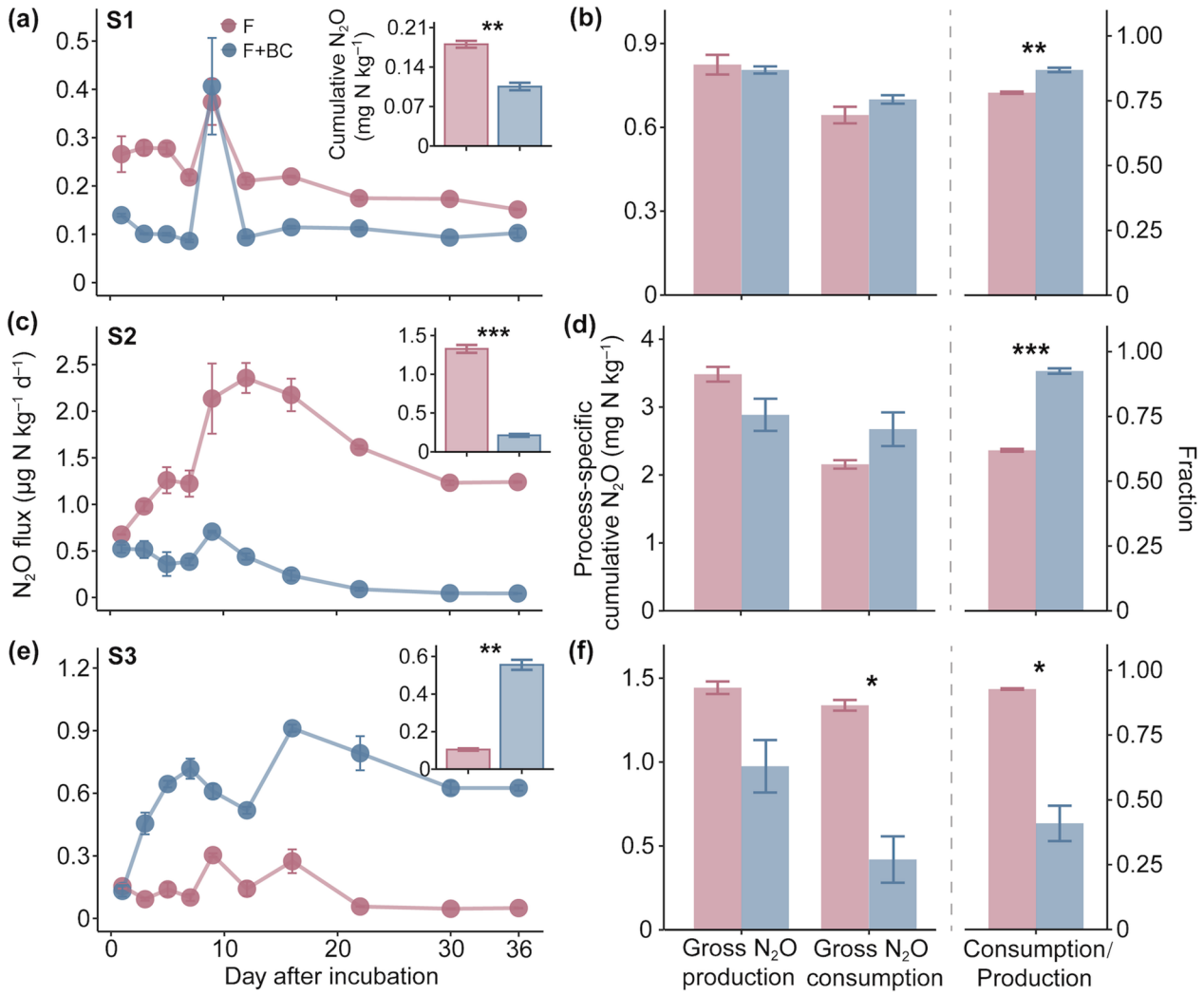


**Fig. 1** Temporal dynamics of soil $N_2O$ fluxes (**a**, **c**, **e**) and gross $N_2O$ production and consumption (**b**, **d**, **f**) during the incubation period at the S1 (**a**, **b**), S2 (**c**, **d**), and S3 (**e**, **f**) sites. Insets show cumulative $N_2O$ emissions. Consumption/Production refers to the ratio of gross $N_2O$ consumption to gross $N_2O$ production. Values represent means ± standard error (SE, $n = 3$). F: conventional N fertilizer; F + BC: conventional N fertilizer combined with biochar. $^{*}P < 0.05$, $^{**}P < 0.01$, and $^{***}P < 0.001$

revealed consistent trends in $N_2O$ reduction between the F and F + BC treatments.

### 3.4 Potential nitrification and denitrification

The legacy effects of biochar significantly affected soil nitrification processes across all sites (Fig. 3). Biochar application increased the total PNR but reduced the $N_2O$ production rate driven by nitrification. Biochar enhanced the rate of heterotrophic nitrification and its contribution to the total PNR (Figs. 3 and S2). Conversely, biochar decreased the contribution of AOB to the total PNR and the rate of AOB-driven $N_2O$ production across all sites. At the S1 and S3 sites, biochar reduced $N_2O$ production from both heterotrophic nitrifiers and AOA (Fig. 3b, f). At the S2 site, in contrast, biochar increased $N_2O$ production from heterotrophic nitrification but decreased AOA-driven emissions (Fig. 3d).

Regarding denitrification, biochar caused a slight increase in the PDR and a reduction in the $N_2O/(N_2O + N_2)$ ratio at the S1 and S2 sites (Fig. 4). In contrast, at the S3 site, biochar significantly reduced PDR and increased the $N_2O/(N_2O + N_2)$ ratio.

### 3.5 Abundance of 16S rRNA and N-cycling genes

The legacy effects of biochar altered the abundances of both 16S rRNA and N-cycling genes. At the S1 and S2 sites, biochar significantly increased the abundance of the 16S rRNA gene, but it decreased at the S3 site (Fig. S3).

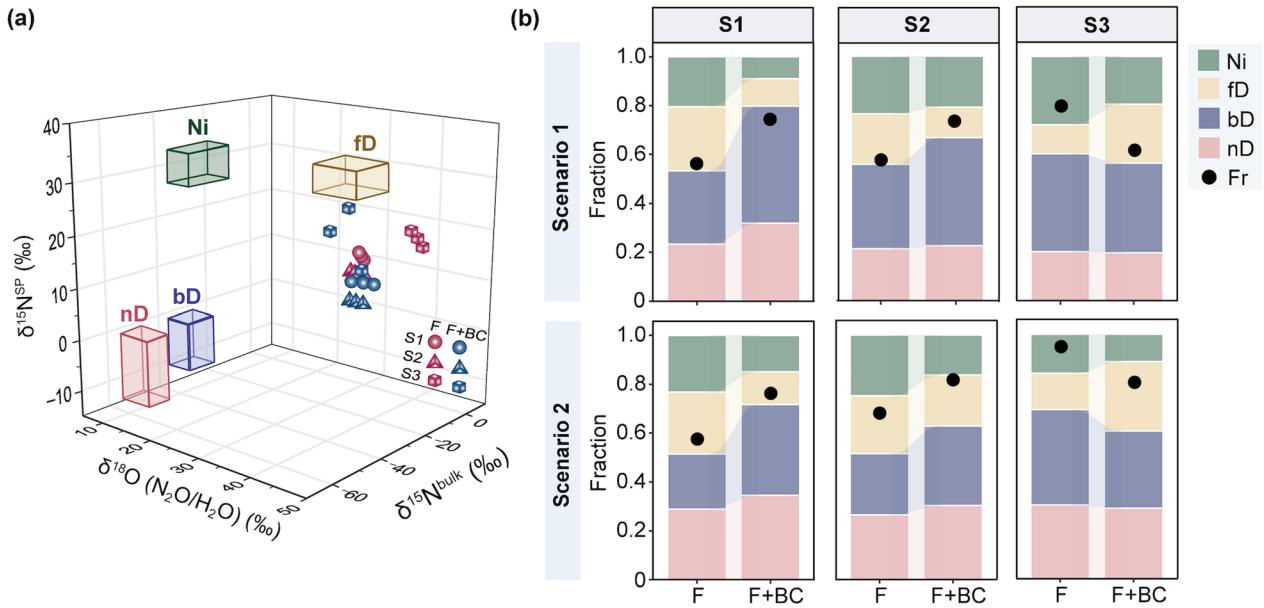


**Fig. 2** Three-dimensional isotopocule plot showing $\delta^{15}N^{SP}$, $\delta^{18}O$, and $\delta^{15}N^{bulk}$ (**a**). Contributions of four microbial pathways to $N_2O$ production and the extent of $N_2O$ reduction (Fr) under two scenarios: Scenario 1 ($N_2O$ from bD is partially reduced before mixing) and Scenario 2 ($N_2O$ from all pathways is mixed before reduction) at the three sites (**b**). The $\delta^{18}O$ values of bD, nD, and fD endmembers were corrected using $\delta^{18}O$-$H_2O$. Ni: nitrification; bD: bacterial denitrification; fD: fungal denitrification; nD: nitrifier denitrification; Fr: the ratio of $N_2O$ reduction. F and F + BC treatments as in Fig. 1

Regarding N-cycling genes, at the S1 site, biochar application led to increased abundance of multiple functional genes, notably *ure*C, *nir*K + *nir*S, and *nos*Z genes (Fig. 5a and d). At the S2 site, biochar significantly enhanced the abundance of AOA, hao, *nir*K, and *nos*Z, whereas it suppressed *gdh*A and *nap*A (Fig. 5b). Additionally, the combined abundance of AOA + AOB, *nir*K + *nir*S, and the *nos*Z/(*nir*K + *nir*S) ratio were increased (Fig. 5e). At the S3 site, biochar increased the abundance of *ure*C, *gdh*A, and AOB, but substantially decreased the abundance of *hao*, *nxr*A, *nar*G, *nap*A, *nir*K, *nir*S, *hzs*B, *nos*Z, and *nif*H (Fig. 5c). These changes were accompanied by a substantial reduction in the abundance of *nir*K + *nir*S and the *nos*Z/(*nir*K + *nir*S) ratio, and by an increase in the abundance of AOA + AOB (Fig. 5f).

### 3.6 Bacterial community and co-occurrence network

The legacy effects of biochar did not significantly alter bacterial alpha diversity across the three sites (Table S3). At the phylum level, the bacterial communities were dominated by Proteobacteria, Actinobacteria, Acidobacteriota, Chloroflexi, and Firmicutes, collectively accounting for more than 80% of total relative abundance under all treatments (Fig. S4).

Co-occurrence networks were constructed for each site (Fig. 6a, c, e). From these, 6, 7, and 5 major modules (containing > 20 nodes) were identified for S1, S2, and S3, respectively (Fig. 6b, d, f). Among these, Module 1 at the S1 and S3 sites and Module 5 at the S2 site showed significantly correlations with cumulative $N_2O$ emissions and differed significantly in abundance between F and F + BC treatments (Figs. 6b, d, f and S5). These modules were selected for further genus-level analysis. At the S1 site, biochar significantly enriched the genera *Rhodanobacter* and *Sphaerobacter*, while decreasing the relative abundance of *Sporosarcina*, *Nitrolancea*, *Bacillus*, *Candidimonas*, and *Chujaibacter* within Module 1 (Fig. 6g). At the S2 site, biochar enriched the relative abundance of *Gemmatimonas*, *Mycobacterium*, *Rhodococcus*, *Nitrospira*, *Bryobacter*, and *Candidatus Solibacter* within Module 5 (Fig. 6h). At the S3 site, biochar increased *Conexibacter*, *Acidibacter*, and *Acidicapsa*, but suppressed *Sphingomonas*, *Acidothermus*, and *Candidatus Solibacter* (Fig. 6i).

## 4 Discussion

### 4.1 Divergent legacy effects of biochar on soil $N_2O$ emissions

Our results demonstrated that the legacy effects of biochar on soil $N_2O$ emissions varied markedly across sites (Fig. 1). Specifically, biochar application 3 and 5 years prior (at the S1 and S2 sites, respectively) significantly reduced $N_2O$ emissions, while biochar applied 9 years earlier (S3 site) resulted in a pronounced increase.

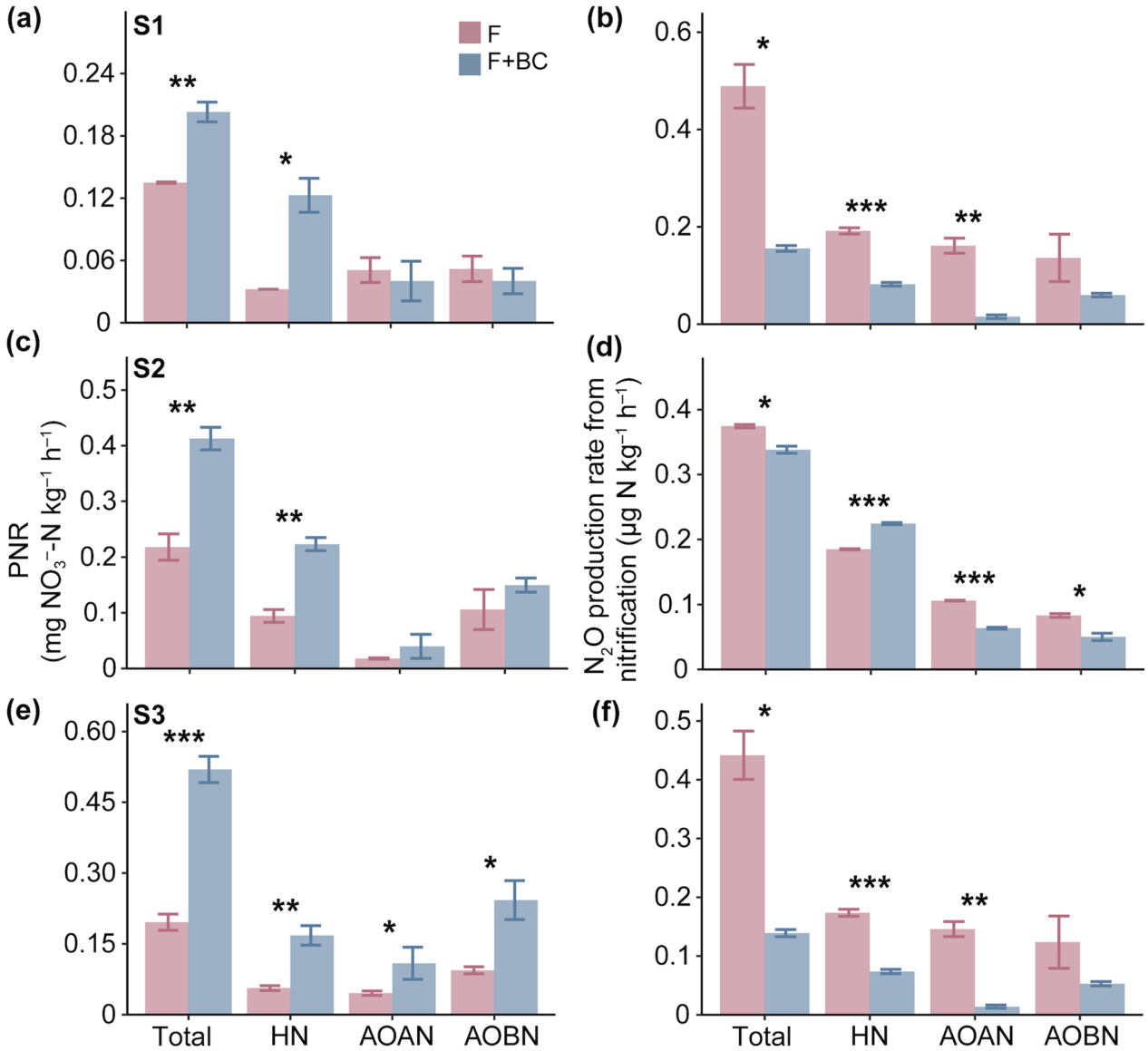


**Fig. 3** Potential nitrification rate (**a**, **c**, **e**) and corresponding $N_2O$ production rate (**b**, **d**, **f**) at the S1 (**a**, **b**), S2 (**c**, **d**), and S3 (**e**, **f**) sites. Total: total nitrification; HN: heterotrophic nitrification; AOAN: nitrification driven by ammonia-oxidizing archaea (AOA); AOBN: nitrification driven by ammonia-oxidizing bacteria (AOB). Values represent means ± SE ($n = 3$). $^{*}P < 0.05$, $^{**}P < 0.01$, and $^{***}P < 0.001$. F and F + BC treatments as in Fig. 1

Notably, biochar significantly reduced $N_2O$ emissions at all sites during the first year after application, as evidenced by unpublished data from the S1 site and our previous findings from the S2 and S3 sites (Ji et al. 2020; Han et al. 2021). These findings indicate that the mitigation effect of biochar on $N_2O$ emissions is not necessarily sustained over time, thereby challenging the assumption of persistent climate benefits. This contradicts our initial hypothesis, which anticipated consistent mitigation across legacy periods. Our short-term findings agree with previous studies reporting that biochar can continue to suppress $N_2O$ emissions several years after application in acidic soils (Wang et al. 2021; Zhang et al. 2021). In contrast, the long-term increase in $N_2O$ emissions observed at the S3 site is consistent with previous studies, which have reported that biochar aging can alter its properties, such as increasing surface acidity and reducing porosity (Duan et al. 2018; Zhang et al. 2019; Wang et al. 2020). These changes may in turn modify soil properties and microbial community composition, thereby affecting N transformations, potentially weakening the mitigation effect, and even leading to enhanced $N_2O$ emissions.

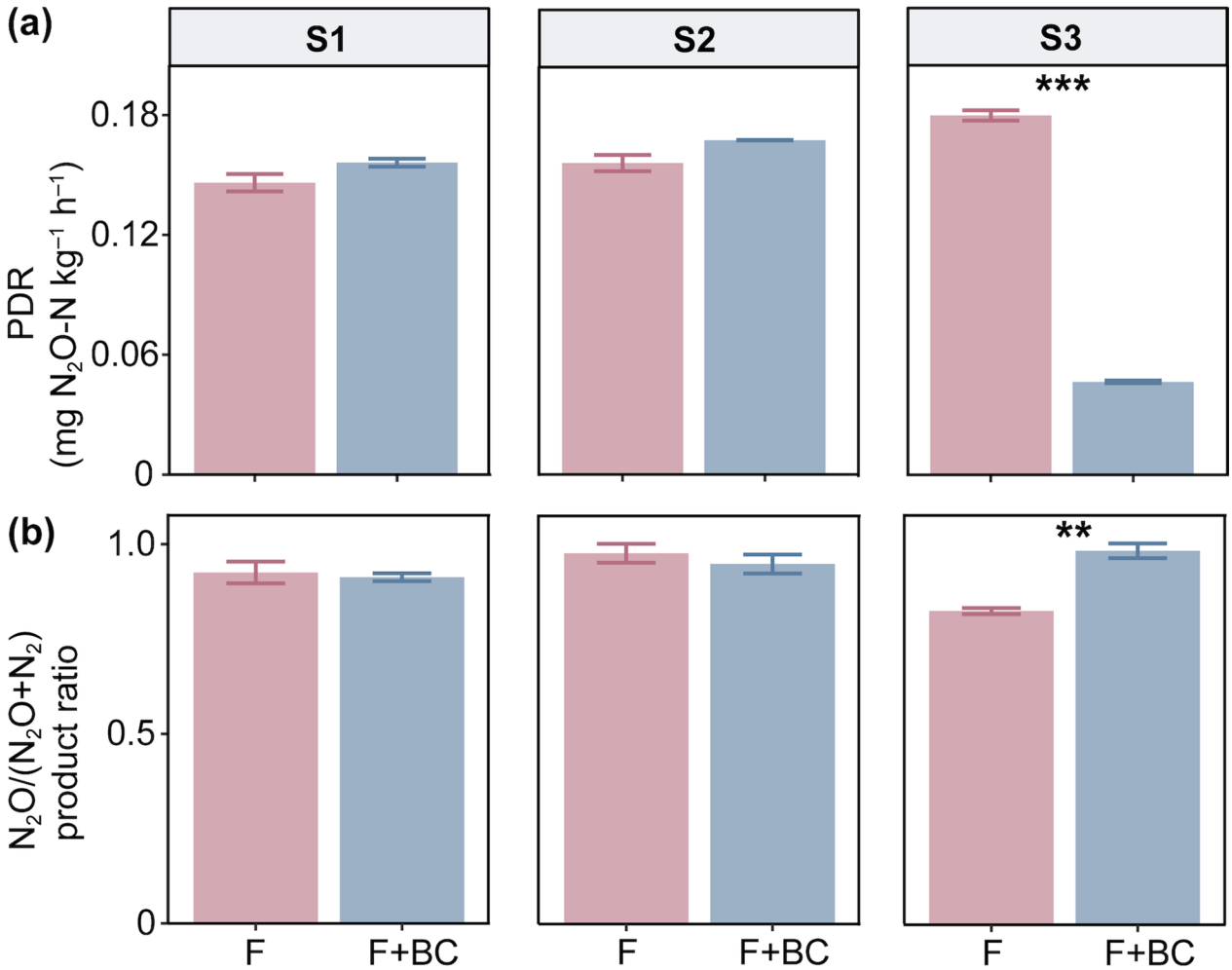


**Fig. 4** Potential denitrification rate (**a**) and the ratio of denitrification end products (**b**) at the three sites. Values represent means ± SE ($n = 3$). $^{*}P < 0.05$, $^{**}P < 0.01$, and $^{***}P < 0.001$. F and F + BC treatments as in Fig. 1

Taken together, these results highlight that the legacy effects of biochar are time-dependent, with the potential to reverse direction over time. The divergent outcomes are likely driven by temporal changes in soil properties, N transformation processes, and microbial community composition. It should be noted, however, that the three study sites differed in soil type and management regime, and therefore do not constitute a strict temporal sequence. The legacy effects reported here should thus be interpreted as site-specific outcomes under their respective conditions, rather than as a direct chronosequence comparison.

### 4.2 Legacy effects of biochar reduce soil $N_2O$ emissions

The short-term legacy effects of biochar significantly reduced soil $N_2O$ emissions (Fig. 1a, c), likely through two primary mechanisms: inhibition of $N_2O$ production and enhancement of $N_2O$ reduction. First, biochar markedly enhanced total PNR, potentially due to increased *ure*C gene abundance. Previous studies have demonstrated that the *ure*C gene is widely used as a functional marker for assessing urea hydrolysis in soils (Mobley et al. 1995; Fisher et al. 2017; Oshiki et al. 2018; Liu et al. 2021). Therefore, its increased abundance may indicate facilitated urea hydrolysis, thereby increasing the availability of substrates for nitrifiers. Interestingly, despite higher PNR, biochar significantly reduced $N_2O$ production rate from nitrification. This apparent contradiction can be explained by two concurrent effects (1) an increased contribution of heterotrophic nitrification (Fig. S2), which generates less $N_2O$ than autotrophic pathways; and (2) a reduced contribution of AOB, which typically produce more $N_2O$ than AOA (Zhang et al. 2015; Hink et al. 2017).

Second, biochar significantly increased the abundance of *nos*Z gene at both the S1 and S2 sites. Concurrently,

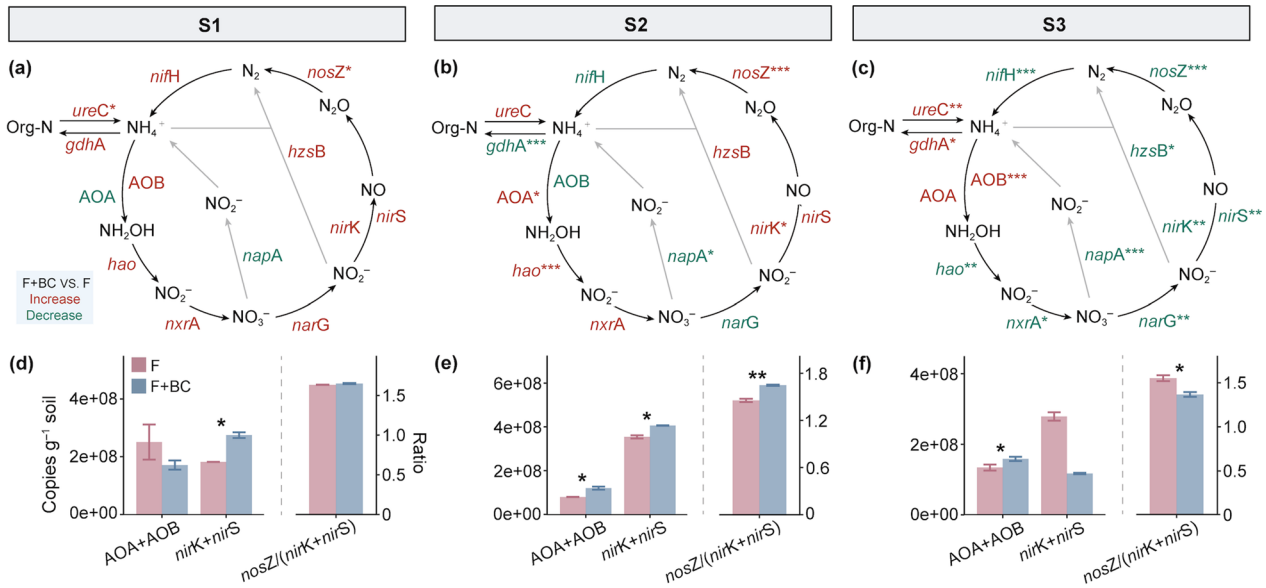


**Fig. 5** The abundances of N-cycling genes at the S1 (**a**, **d**), S2 (**b**, **e**), and S3 (**c**, **f**) sites. In (**a**–**c**), red denotes higher gene abundance, whereas green represents lower gene abundance in the F + BC treatment relative to the F treatment. Values represent means ± SE ($n = 3$). $^{*}P < 0.05$, $^{**}P < 0.01$, and $^{***}P < 0.001$. F and F + BC treatments as in Fig. 1

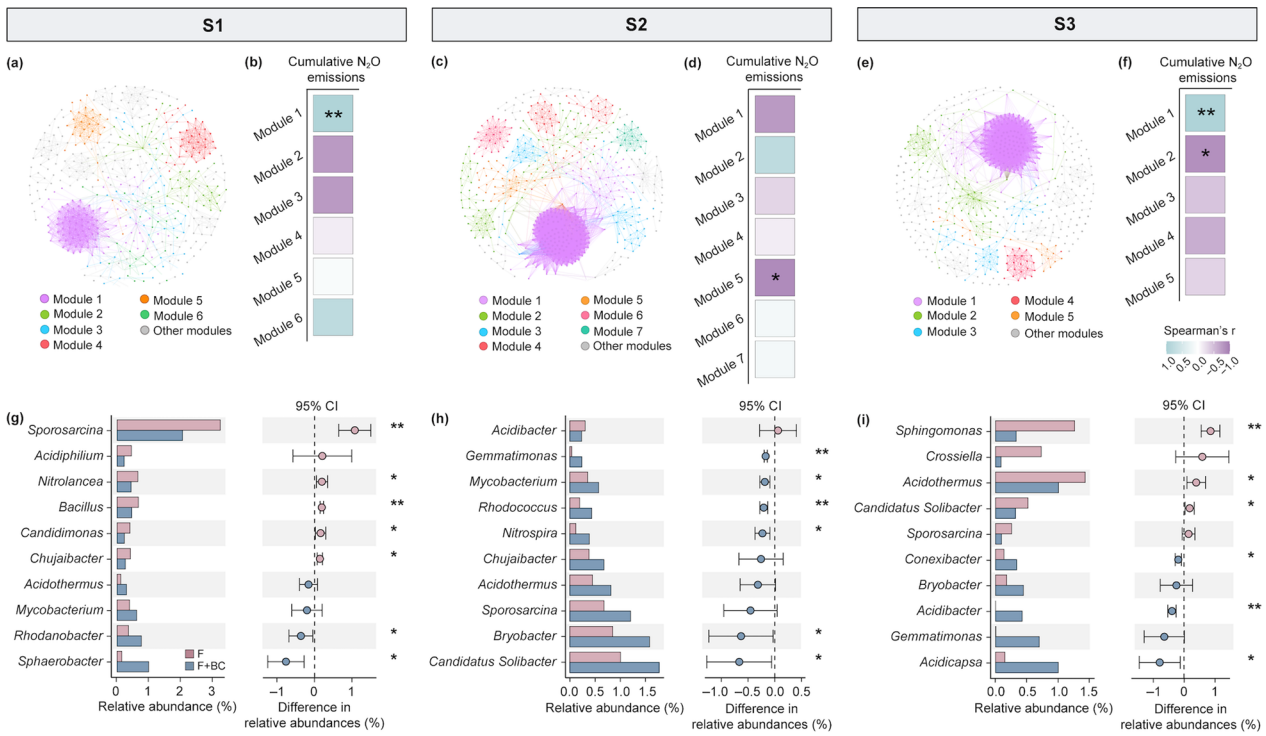


**Fig. 6** Co-occurrence network analysis of soil bacteria at the S1 (**a**, **b**, **g**), S2 (**c**, **d**, **h**), and S3 (**e**, **f**, **i**) sites. Microbial network of soil bacteria across F and F + BC treatments at each site (**a**, **c**, **e**). The network is divided into several sub-networks, referred to as modules, which are clusters of closely interconnected nodes. Spearman's rank correlations between the relative abundance of the main modules and the cumulative $N_2O$ emissions (**b**, **d**, **f**). The color gradient represents Spearman's correlation coefficients. STAMP analysis revealed differences in the relative abundance of the top 10 genera between F and F + BC treatments within Module 1 at the S1 and S3 sites, and within Module 5 at the S2 site (**g**-**i**). These modules were significantly correlated with the cumulative $N_2O$ emissions and exhibited significant differences between treatments (Fig. S5). F and F + BC treatments as in Fig. 1. $^{*}P < 0.05$, $^{**}P < 0.01$, and $^{***}P < 0.001$

biochar enriched genera carrying the *nos*Z gene, including *Rhodanobacter* (S1) and *Gemmatimonas* (S2) (Fig. 6g, h), both of which are capable of reducing $N_2O$ to $N_2$ (Hallin et al. 2018; Bano et al. 2024). These shifts were positively correlated with gross $N_2O$ consumption and negatively correlated with cumulative $N_2O$ emissions (Fig. S6). At the S1 site, increased soil pH likely contributed to the stimulation of $N_2O$-reducing bacteria, as neutral-to-alkaline conditions favor the expression of *nos*Z genes (Xu et al. 2014). Moreover, biochar increased DOC and the *nos*Z/(*nir*K + *nir*S) ratio at both sites, further supporting promoted denitrification completeness (Fig. 1 and 5d, e). This is attributable to DOC serving as an essential carbon source and electron donor for denitrifiers (McCarty and Bremner 1992; Kuypers et al. 2018; Fu et al. 2022), and greater DOC availability likely facilitated the reduction of $N_2O$ to $N_2$. Additionally, biochar increased the contribution of bacterial denitrification while reducing that of fungal denitrification to $N_2O$ production, potentially explaining the observed increase in $N_2O$ reduction (Fig. 2b). This shift is critical, as fungal denitrifiers lack *nos*Z, and thus their denitrification typically terminates at $N_2O$ rather than $N_2$ (Lycus et al. 2018; Shan et al. 2021). Together, these findings demonstrate that the short-term legacy effects of biochar suppress nitrification-derived $N_2O$ emissions and promote $N_2O$ reduction through enhanced microbial potential and carbon availability, resulting in a net mitigation effect.

### 4.3 Legacy effects of biochar increase soil $N_2O$ emissions

At the S3 site (9 years after biochar application), the legacy effects of biochar led to a significant increase in $N_2O$ emissions (Fig. 1e), contrary to its initial mitigation effect. This increase can be attributed to an imbalance between reduced $N_2O$ production and even more strongly suppressed $N_2O$ reduction (Fig. 1f). Biochar significantly increased *ure*C gene abundance (Fig. 5c), which is consistent with a previous study (Liu et al. 2021). Given that the *ure*C gene is widely recognized as a functional marker for soil urea hydrolysis (Oshiki et al. 2018), its increased abundance potentially promotes urea hydrolysis and enhances ammonia supply for nitrification. Accordingly, total PNR was increased (Fig. 3e). However, despite the increased nitrification potential, total nitrification-derived $N_2O$ production declined, consistent with an increased contribution of heterotrophic nitrification and a decreased role of AOB (Fig. S2, Fig. 3e, f). These changes suggest that biochar suppressed high-emission autotrophic pathways while favoring lower-emission heterotrophic ones.

Biochar significantly increased soil $NO_3^-$-N concentration, likely driven by enhanced PNR. Yet, denitrification activity was weakened: PDR decreased markedly, and the $N_2O/(N_2O + N_2)$ ratio rose sharply (Fig. 4c). This was accompanied by reduced *nir*K, *nir*S, and *nos*Z gene abundances, as well as lower DOC content. As denitrification is a heterotrophic, carbon-dependent process, the reduction in available DOC likely limited electron donors for complete denitrification, thereby promoting $N_2O$ accumulation (McCarty and Bremner 1992; Kuypers et al. 2018). The decline in DOC may be partially explained by the reduced abundance of genera such as *Sphingomonas* and *Candidatus Solibacter*, both known for their roles in degrading organic matter (Lee et al. 2011; Rime et al. 2015). These genera were positively correlated with DOC content (Fig. S6), supporting their functional link to carbon cycling.

Although biochar is typically alkaline, its long-term legacy effects at S3 site led to a significant decline in soil pH as reported previously (Wang et al. 2020; Guo et al. 2022), likely due to the accumulation of acidic functional groups on aged biochar surfaces (Mukherjee et al. 2014; Liu et al. 2019). This acidification may have further inhibited *nos*Z gene expression and the activity of $N_2O$-reducing bacteria (Hallin et al. 2018; Qiu et al. 2024), consistent with the observed decline in $N_2O$ consumption and *nos*Z/(*nir*K + *nir*S) ratio (Figs. 1f and 4). Isotopic analysis supported this conclusion, that is, biochar decreased the contribution of bacterial denitrification and increased the role of fungal denitrification, which lacks the capacity to reduce $N_2O$ to $N_2$ (Fig. 2b; Mothapo et al. 2015). This microbial shift likely contributed to elevated $N_2O$ emissions despite reduced production rates. Collectively, these results demonstrate that while the long-term legacy effects of biochar may suppress $N_2O$ production pathways, its stronger inhibition of $N_2O$ reduction, driven by microbial, chemical, and carbon constraints, ultimately leads to increased $N_2O$ emissions.

## 5 Conclusions

This study demonstrates that the legacy effects of biochar on $N_2O$ emissions in acidic soils are both time-dependent and directionally divergent. In the short term (3- and 5-years post-application), biochar significantly reduced $N_2O$ emissions by inhibiting nitrification-derived $N_2O$ production and enhancing microbial $N_2O$ reduction. These effects were associated with increased heterotrophic nitrification, elevated *nos*Z gene abundance, and enrichment of $N_2O$-reducing taxa such as *Rhodanobacter* and *Gemmatimonas*. In contrast, long-term legacy effects of biochar (9 years) led to increased $N_2O$ emissions, as $N_2O$ reduction was more strongly inhibited than production. This shift was associated with reduced *nos*Z abundance, lower DOC availability, microbial community restructuring, soil acidification, and an increased contribution of fungal denitrification lacking the capacity to

reduce $N_2O$ to $N_2$. These findings highlight that the mitigation potential of biochar cannot be assumed to persist indefinitely and may even reverse over time. Long-term impacts should therefore be explicitly considered when evaluating biochar as a climate mitigation strategy. Future research should focus on long-term field monitoring across diverse soils, climates, and cropping systems, and on identifying strategies, such as targeted amendments or microbial interventions, to sustain or restore the suppressive effect of biochar on $N_2O$ emissions.

## Supplementary Information

The online version contains supplementary material available at https://doi.org/10.1007/s42773-025-00558-9.

Supplementary file 1.

### Author contributions

Shumin Guo: Conceptualization, formal analysis, methodology, experimental operation, visualization, writing-original draft. Haiyan Lin: Experimental operation, writing-reviewing and editing; Zhutao Li: Experimental operation, writing-review and editing; Zhaoqiang Han, Jie Wu, Xiaomeng Bo, Mengxue Shen, Zhiwei Zhang, Shuwei Liu: Writing-review and editing; Jinyang Wang: Conceptualization, supervision, funding acquisition, writing-reviewing and editing; Jianwen Zou: Conceptualization, supervision, writing-reviewing and editing. All authors read and approved the final manuscript.

### Funding

This study was supported by the National Natural Science Foundation of China (42477358, 42407472, 42177285) and the Fundamental Research Funds for the Central Universities (KJYQ2025037). This research was partially supported by the initiative advancing dual certification for eco-friendly premium agricultural products and carbon footprint assessment.

### Data availability

The datasets used or analyzed in this study are available from the corresponding author upon reasonable request.

## Declarations

### Competing interests

The authors have no relevant financial or non-financial interests to disclose.

### Author details

[1]Key Laboratory of Agricultural Green and Low-Carbon in Southeastern China, Ministry of Agriculture and Rural Affairs, Nanjing Agricultural University, Nanjing 210095, Jiangsu, China. [2]College of Resources and Environmental Sciences, Nanjing Agricultural University, Nanjing 210095, Jiangsu, China. [3]Jiangsu Key Laboratory of Low Carbon Agriculture and GHGs Mitigation, Jiangsu Collaborative Innovation Center for Solid Organic Waste Resource Utilization, Nanjing 210095, Jiangsu, China.

Received: 21 June 2025 Revised: 20 November 2025 Accepted: 8 December 2025
Published online: 03 February 2026

### References

Ameloot N, De Neve S, Jegajeevagan K, Yildiz G, Buchan D, Funkuin YN, Prins W, Bouckaert L, Sleutel S (2013) Short-term $CO_2$ and $N_2O$ emissions and microbial properties of biochar amended sandy loam soils. Soil Biol Biochem 57:401–410. https://doi.org/10.1016/j.soilbio.2012.10.025

Bano S, Wu Q, Yu S, Wang X, Zhang X (2024) Soil properties drive nitrous oxide accumulation patterns by shaping denitrifying bacteriomes. Environ Microbiome. https://doi.org/10.1186/s40793-024-00643-9

Bo X, Zhang Z, Wang J, Guo S, Li Z, Lin H, Huang Y, Han Z, Kuzyakov Y, Zou J (2023) Benefits and limitations of biochar for climate-smart agriculture: a review and case study from China. Biochar. https://doi.org/10.1007/s42773-023-00279-x

Buchen C, Lewicka-Szczebak D, Flessa H, Well R (2018) Estimating $N_2O$ processes during grassland renewal and grassland conversion to maize cropping using $N_2O$ isotopocules. Rapid Commun Mass Spectrom 32:1053–1067. https://doi.org/10.1002/rcm.8132

Callahan BJ, McMurdie PJ, Rosen MJ, Han AW, Johnson AJA, Holmes SP (2016) DADA2: High-resolution sample inference from Illumina amplicon data. Nat Methods 13:581–583. https://doi.org/10.1038/nmeth.3869

Carter, M.R., Gregorich, E.G. (2007). Soil Sampling and Methods of Analysis, second ed. CRC Press, Boca Raton, FL. https://doi.org/10.1201/9781420005271.

Cayuela ML, van Zwieten L, Singh BP, Jeffery S, Roig A, Sánchez-Monedero MA (2014) Biochar's role in mitigating soil nitrous oxide emissions: a review and meta-analysis. Agric Ecosyst Environ 191:5–16. https://doi.org/10.1016/j.agee.2013.10.009

Chen W, Meng J, Han X, Lan Y, Zhang W (2019) Past, present, and future of biochar. Biochar 1:75–87. https://doi.org/10.1007/s42773-019-00008-3

Coplen TB (2011) Guidelines and recommended terms for expression of stable- isotope-ratio and gas-ratio measurement results. Rapid Commun Mass Spectrom 25:2538–2560. https://doi.org/10.1002/rcm.5129

Delgado-Baquerizo M, Reith F, Dennis PG, Hamonts K, Powell JR, Young A, Singh BK, Bissett A (2018) Ecological drivers of soil microbial diversity and soil biological networks in the Southern Hemisphere. Ecology 99:583–596. https://doi.org/10.1002/ecy.2137

Dong X, Li G, Lin Q, Zhao X (2017) Quantity and quality changes of biochar aged for 5 years in soil under field conditions. CATENA 159:136–143. https://doi.org/10.1016/j.catena.2017.08.008

Duan P, Zhang X, Zhang Q, Wu Z, Xiong Z (2018) Field-aged biochar stimulated $N_2O$ production from greenhouse vegetable production soils by nitrification and denitrification. Sci Total Environ 642:1303–1310. https://doi.org/10.1016/j.scitotenv.2018.06.166

Duan P, Zhou J, Feng L, Jansen-Willems AB, Xiong Z (2019) Pathways and controls of $N_2O$ production in greenhouse vegetable production soils. Biol Fertil Soils 55:285–297. https://doi.org/10.1007/s00374-019-01348-9

Fisher KA, Yarwood SA, James BR (2017) Soil urease activity and bacterial ureC gene copy numbers: effect of pH. Geoderma 285:1–8. https://doi.org/10.1016/j.geoderma.2016.09.012

Fu X, Hou R, Yang P, Qian S, Feng Z, Chen Z, Wang F, Yuan R, Chen H, Zhou B (2022) Application of external carbon source in heterotrophic denitrification of domestic sewage: a review. Sci Total Environ 817:153061. https://doi.org/10.1016/j.scitotenv.2022.153061

Guo S, Wu J, Han Z, Li Z, Xu P, Liu S, Wang J, Zou J (2022) The legacy effect of biochar application on soil nitrous oxide emissions. GCB Bioenergy 15:478–493. https://doi.org/10.1111/gcbb.13022

Hagemann N, Harter J, Kaldamukova R, Guzman-Bustamante I, Ruser R, Graeff S, Kappler A, Behrens S (2017) Does soil aging affect the $N_2O$ mitigation potential of biochar? A combined microcosm and field study. GCB Bioenergy 9:953–964. https://doi.org/10.1111/gcbb.12390

Hallin S, Philippot L, Löffler FE, Sanford RA, Jones CM (2018) Genomics and ecology of novel $N_2O$-reducing microorganisms. Trends Microbiol 26:43–55. https://doi.org/10.1016/j.tim.2017.07.003

Han Z, Wang J, Xu P, Li Z, Liu S, Zou J (2021) Differential responses of soil nitrogen-oxide emissions to organic substitution for synthetic fertilizer and biochar amendment in a subtropical tea plantation. GCB Bioenergy 13:1260–1274. https://doi.org/10.1111/gcbb.12842

Hart, S.C., Stark, J.M., Davidson, E.A., Firestone, M.K. Nitrogen Mineralization, Immobilization, and Nitrification. 1994; 985–1018. https://doi.org/10.2136/sssabookser5.2.c42.

Heil J, Liu S, Vereecken H, Brüggemann N (2015) Abiotic nitrous oxide production from hydroxylamine in soils and their dependence on soil properties. Soil Biol Biochem 84:107–115. https://doi.org/10.1016/j.soilbio.2015.02.022

Hink L, Nicol GW, Prosser JI (2017) Archaea produce lower yields of $N_2O$ than bacteria during aerobic ammonia oxidation in soil. Environ Microbiol 19:4829–4837. https://doi.org/10.1111/1462-2920.13282

Ji C, Li S, Geng Y, Yuan Y, Zhi J, Yu K, Han Z, Wu S, Liu S, Zou J (2020) Decreased $N_2O$ and NO emissions associated with stimulated denitrification following biochar amendment in subtropical tea plantations. Geoderma 365:114223. https://doi.org/10.1016/j.geoderma.2020.114223
Jones CM, Putz M, Tiemann M, Hallin S (2022) Reactive nitrogen restructures and weakens microbial controls of soil $N_2O$ emissions. Commun Biol 5:273. https://doi.org/10.1038/s42003-022-03211-4
Krause HM, Hüppi R, Leifeld J, El-Hadidi M, Harter J, Kappler A, Hartmann M, Behrens S, Mäder P, Gattinger A (2018) Biochar affects community composition of nitrous oxide reducers in a field experiment. Soil Biol Biochem 119:143–151. https://doi.org/10.1016/j.soilbio.2018.01.018
Kuypers MMM, Marchant HK, Kartal B (2018) The microbial nitrogen-cycling network. Nat Rev Microbiol 16:263–276. https://doi.org/10.1038/nrmicro.2018.9
Lee CG, Watanabe T, Sato Y, Murase J, Asakawa S, Kimura M (2011) Bacterial populations assimilating carbon from $^{13}$C-labeled plant residue in soil: analysis by a DNA-SIP approach. Soil Biol Biochem 43:814–822. https://doi.org/10.1016/j.soilbio.2010.12.016
Lewicka-Szczebak D, Piotr Lewicki M, Well R (2020) $N_2O$ isotope approaches for source partitioning of $N_2O$ production and estimation of $N_2O$ reduction-validation with the $^{15}$N gas-flux method in laboratory and field studies. Biogeosciences 17:5513–5537. https://doi.org/10.5194/bg-17-5513-2020
Lewicki MP, Lewicka-Szczebak D, Skrzypek G (2022) FRAME—Monte carlo model for evaluation of the stable isotope mixing and fractionation. PLoS ONE 17:4–7. https://doi.org/10.1371/journal.pone.0277204
Liao X, Liu D, Niu Y, Chen Z, He T, Ding W (2021) Effect of field-aged biochar on fertilizer N retention and $N_2O$ emissions: a field microplot experiment with $^{15}$N-labeled urea. Sci Total Environ 773:145645. https://doi.org/10.1016/j.scitotenv.2021.145645
Lin Y, Ding W, Liu D, He T, Yoo G, Yuan J, Chen Z, Fan J (2017) Wheat straw-derived biochar amendment stimulated $N_2O$ emissions from rice paddy soils by regulating the amoA genes of ammonia-oxidizing bacteria. Soil Biol Biochem 113:89–98. https://doi.org/10.1016/j.soilbio.2017.06.001
Lin H, Yuan Q, Yu Q, Chen Z, Ma J (2022) Plants mitigate nitrous oxide emissions from antibiotic-contaminated agricultural soils. Environ Sci Technol 56:4950–4960. https://doi.org/10.1021/acs.est.1c06508
Liu Y, Sohi SP, Jing F, Chen J (2019) Oxidative ageing induces change in the functionality of biochar and hydrochar: mechanistic insights from sorption of atrazine. Environ Pollut 249:1002–1010. https://doi.org/10.1016/j.envpol.2019.03.035
Liu Z, Yang E, Lan Y, He T, Chen W, Meng J (2021) Effect of biochar on urea hydrolysis rate and soil ureC gene copy numbers. J Soil Sci Plant Nutr 21:3122–3131. https://doi.org/10.1007/s42729-021-00593-y
Lycus P, Soriano-Laguna MJ, Kjos M, Richardson DJ, Gates AJ, Milligan DA, Frostegård Å, Bergaust L, Bakken LR (2018) A bet-hedging strategy for denitrifying bacteria curtails their release of $N_2O$. Proc Natl Acad Sci U S A 115:11820–11825. https://doi.org/10.1073/pnas.1805000115
McCarty GW, Bremner JM (1992) Availability of organic carbon for denitrification of nitrate in subsoils. Biol Fertil Soils 14:219–222. https://doi.org/10.1007/BF00346064
Mobley HLT, Island MD, Hausinger RP (1995) Molecular biology of microbial ureases. Methods Mol Biol 59:451–480. https://doi.org/10.1007/978-1-0716-2329-9_2
Mothapo N, Chen H, Cubeta MA, Grossman JM, Fuller F, Shi W (2015) Phylogenetic, taxonomic and functional diversity of fungal denitrifiers and associated $N_2O$ production efficacy. Soil Biol Biochem 83:160–175. https://doi.org/10.1016/j.soilbio.2015.02.001
Mukherjee A, Zimmerman AR, Hamdan R, Cooper WT (2014) Physicochemical changes in pyrogenic organic matter (biochar) after 15 months of field aging. Solid Earth 5:693–704. https://doi.org/10.5194/se-5-693-2014
Mushinski RM, Phillips RP, Payne ZC, Abney RB, Jo I, Fei S, Pusede SE, White JR, Rusch DB, Raff JD (2019) Microbial mechanisms and ecosystem flux estimation for aerobic $NO_y$ emissions from deciduous forest soils. Proc Natl Acad Sci U S A 116:2138–2145. https://doi.org/10.1073/pnas.1814632116
Oshiki M, Araki M, Hirakata Y, Hatamoto M, Yamaguchi T, Araki N (2018) Ureolytic prokaryotes in soil: community abundance and diversity. Microbes Environ 33:230–233. https://doi.org/10.1264/jsme2.ME17188
Qiu Y, Zhang Y, Zhang K, Xu X, Zhao Y, Bai T, Zhao Y, Wang H, Sheng X, Bloszies S, Gillespie CJ, He T, Wang Y, Chen H, Guo L, Song H, Ye C, Wang Yi, Woodley A, Guo J (2024) Intermediate soil acidification induces highest nitrous oxide emissions. Nat Commun. https://doi.org/10.1038/s41467-024-46931-3
R Core Team, 2021. A language and environment for statistical computing. R Foundation for Statistical Computing 3, Vienna, Austria. https://www.R-project.org
Ravishankara AR, Daniel JS, Portmann RW (2009) Nitrous oxide ($N_2O$): the dominant ozone-depleting substance emitted in the 21st century. Science 326:123–125. https://doi.org/10.1126/science.1176985
Rime T, Hartmann M, Brunner I, Widmer F, Zeyer J, Frey B (2015) Vertical distribution of the soil microbiota along a successional gradient in a glacier forefield. Mol Ecol 24:1091–1108. https://doi.org/10.1111/mec.13051
Shan J, Sanford RA, Chee-Sanford J, Ooi SK, Löffler FE, Konstantinidis KT, Yang WH (2021) Beyond denitrification: the role of microbial diversity in controlling nitrous oxide reduction and soil nitrous oxide emissions. Glob Change Biol 27:2669–2683. https://doi.org/10.1111/gcb.15545
Tian H, Xu R, Canadell JG, Thompson RL, Winiwarter W, Suntharalingam P et al (2020) A comprehensive quantification of global nitrous oxide sources and sinks. Nature 586:248–256. https://doi.org/10.1038/s41586-020-2780-0
Toyoda S, Yoshida N (1999) Determination of nitrogen isotopomers of nitrous oxide on a modified isotope ratio mass spectrometer. Anal Chem 71:4711–4718. https://doi.org/10.1021/ac9904563
Toyoda S, Yano M, Nishimura S, Akiyama H, Hayakawa A, Koba K, Sudo S, Yagi K, Makabe A, Tobari Y, Ogawa NO, Ohkouchi N, Yamada K, Yoshida N (2011) Characterization and production and consumption processes of $N_2O$ emitted from temperate agricultural soils determined via isotopomer ratio analysis. Glob Biogeochem Cycles 25:n/a-n/a. https://doi.org/10.1029/2009gb003769
Toyoda S, Yoshida N, Koba K (2017) Isotopocule analysis of biologically produced nitrous oxide in various environments. Mass Spectrom Rev 36:135–160. https://doi.org/10.1002/mas.21459
Wang J, Xiong Z, Kuzyakov Y (2016) Biochar stability in soil: meta-analysis of decomposition and priming effects. GCB Bioenergy 8:512–523
Wang Y, Guo J, Vogt RD, Mulder J, Wang J, Zhang X (2018) Soil pH as the chief modifier for regional nitrous oxide emissions: new evidence and implications for global estimates and mitigation. Glob Change Biol 24:e617–e626. https://doi.org/10.1111/gcb.13966
Wang L, O'Connor D, Rinklebe J, Ok YS, Tsang DCW, Shen Z, Hou D (2020) Biochar aging: mechanisms, physicochemical changes, assessment, and implications for field applications. Environ Sci Technol 54:14797–14814. https://doi.org/10.1021/acs.est.0c04033
Wang L, Gao C, Yang K, Sheng Y, Xu J, Zhao Y, Lou J, Sun R, Zhu L (2021) Effects of biochar aging in the soil on its mechanical property and performance for soil $CO_2$ and $N_2O$ emissions. Sci Total Environ 782:146824. https://doi.org/10.1016/j.scitotenv.2021.146824
Well R, Kurganova I, De Gerenyu VL, Flessa H (2006) Isotopomer signatures of soil-emitted $N_2O$ under different moisture conditions - a microcosm study with arable loess soil. Soil Biol Biochem 38:2923–2933. https://doi.org/10.1016/j.soilbio.2006.05.003
Woolf D, Lehmann J, Lee DR (2016) Optimal bioenergy power generation for climate change mitigation with or without carbon sequestration. Nat Commun 7:1–11. https://doi.org/10.1038/ncomms13160
Wu D, Well R, Cárdenas LM, Fuß R, Lewicka-Szczebak D, Köster JR, Brüggemann N, Bol R (2019) Quantifying $N_2O$ reduction to $N_2$ during denitrification in soils via isotopic mapping approach: Model evaluation and uncertainty analysis. Environ Res. https://doi.org/10.1016/j.envres.2019.108806
Xu HJ, Wang XH, Li H, Yao HY, Su JQ, Zhu YG (2014) Biochar impacts soil microbial community composition and nitrogen cycling in an acidic soil planted with rape. Environ Sci Technol 48:9391–9399. https://doi.org/10.1021/es5021058
Yamamoto A, Uchida Y, Akiyama H, Nakajima Y (2014) Continuous and unattended measurements of the site preference of nitrous oxide emitted from an agricultural soil using quantum cascade laser spectrometry with intercomparison with isotope ratio mass spectrometry. Rapid Commun Mass Spectrom 28:1444–1452. https://doi.org/10.1002/rcm.6916
Yang WH, Teh YA, Silver WL (2011) A test of a field-based $^{15}$N-nitrous oxide pool dilution technique to measure gross $N_2O$ production in soil. Glob Change Biol 17:3577–3588. https://doi.org/10.1111/j.1365-2486.2011.02481.x
Yin C, Fan X, Yan G, Chen H, Ye M, Ni L, Peng H, Ran W, Zhao Y, Li T, Wakelin SA, Liang Y (2020) Gross $N_2O$ production process, not consumption, determines the temperature sensitivity of Net $N_2O$ emission in arable

soil subject to different long-term fertilization practices. Front Microbiol. https://doi.org/10.3389/fmicb.2020.00745

Yu L, Harris E, Lewicka-Szczebak D, Barthel M, Blomberg MRA, Harris SJ, Johnson MS, Lehmann MF, Liisberg J, Müller C, Ostrom NE, Six J, Toyoda S, Yoshida N, Mohn J (2020) What can we learn from $N_2O$ isotope data? – analytics, processes and modelling. Rapid Commun Mass Spectrom 34:1–14. https://doi.org/10.1002/rcm.8858

Zhang J, Müller C, Cai Z (2015) Heterotrophic nitrification of organic N and its contribution to nitrous oxide emissions in soils. Soil Biol Biochem 84:199–209. https://doi.org/10.1016/j.soilbio.2015.02.028

Zhang X, Duan P, Wu Z, Xiong Z (2019) Aged biochar stimulated ammonia-oxidizing archaea and bacteria-derived $N_2O$ and NO production in an acidic vegetable soil. Sci Total Environ 687:433–440. https://doi.org/10.1016/j.scitotenv.2019.06.128

Zhang Q, Zhang X, Duan P, Jiang X, Shen H, Yan X, Xiong Z (2021) The effect of long-term biochar amendment on $N_2O$ emissions: experiments with $^{15}N$–$^{18}O$ isotopes combined with specific inhibition approaches. Sci Total Environ 769:144533. https://doi.org/10.1016/j.scitotenv.2020.144533

Zheng B, Zhu Y, Sardans J, Peñuelas J, Su J (2018) QMEC: a tool for high-throughput quantitative assessment of microbial functional potential in C, N, P, and S biogeochemical cycling. Sci China Life Sci 61:1451–1462. https://doi.org/10.1007/s11427-018-9364-7

Zou J, Huang Y, Qin Y, Liu S, Shen Q, Pan G, Lu Y, Liu Q (2009) Changes in fertilizer-induced direct $N_2O$ emissions from paddy fields during rice-growing season in China between 1950s and 1990s. Glob Change Biol 15:229–242. https://doi.org/10.1111/j.1365-2486.2008.01775.x